Dynamics of atomic sublevel coherences during modulated optical pumping

Dieter Suter
Institute of Quantum Electronics, Swiss Federal Institute of Technology (EidgenössischeTechnische Hochschule) Zürich, CH-8093 Zürich, Switzerland

Jürgen Mlynek
Department of Physics, Universität Konstanz, D-7750 Konstanz, Germany
(Received 9 November 1990)

The dynamics of coherences between sublevels of an electronic ground state is investigated under conditions of modulated optical pumping. It is shown that the modulation corresponds to an effective reduction of the apparent sublevel splitting, thereby allowing the excitation of coherences between atomic sublevels whose energy splitting would require very high laser intensities for dc excitation. In addition, the frequency and phase of the modulation introduce additional degrees of freedom that can be utilized for the design of new experiments. The theoretical evaluations are compared with experiments on the ground state of atomic sodium.

I. INTRODUCTION

The excitation of sublevel coherences with pulses of polarized light is an efficient method for the spectroscopy of atomic sublevels.[1] A typical experimental setup, as shown schematically in Fig. 1, uses a laser beam that interacts with an electronic transition of the atomic medium. If the laser beam is suitably polarized, it can transfer angular momentum from the photons to the atomic medium, thereby creating anisotropy in the state of the atoms. In the example shown, the pump laser beam is circularly polarized. A second laser beam is used to detect the orientation present in the sample cell via polarization-selective detection of the transmitted light. For time-resolved experiments, optical pulses can be used, derived either from a pulsed laser system or by external modulation, as shown in the figure.

In the case of transverse optical pumping, i.e., when the direction of the laser beam is perpendicular to the direction of the magnetic field, efficient excitation of ground-state sublevel coherences requires that the optical pumping rate be large compared to the Larmor frequency.[1-4] If the sublevel splitting becomes large, the dephasing time of the optical coherences is short, or the optical irradiation is far from resonance, this requirement can pose severe requirements on the laser intensity.

On the other hand, it was realized early[5] that if the intensity of the light is modulated at a frequency near the Larmor frequency of the system, it is possible to excite coherence between atomic sublevels with relatively low light intensities. These early experiments were performed with harmonic modulation of a continuous light source, a technique which is still applied today.[6,7] With the introduction of pulsed laser systems, however, it became also attractive to use trains of short equidistant pulses.[8] This technique has been extended to very high frequencies recently[9] and thereby made it possible to detect sublevel splittings in the GHz region.

Most of these experiments were performed in the frequency domain by scanning either the modulation frequency or the frequency of the sublevel splitting by varying the strength of the magnetic field, while keeping the other quantity constant. A few time-domain experiments, such as the creation of spin echoes, have also used modulation of the laser intensity.[10] This experiment demonstrated that modulation of the laser intensity not only leads to more efficient optical pumping, but that also the efficiency of the light shift effect, which is responsible for the echo formation,[11] is improved at higher sublevel splittings.

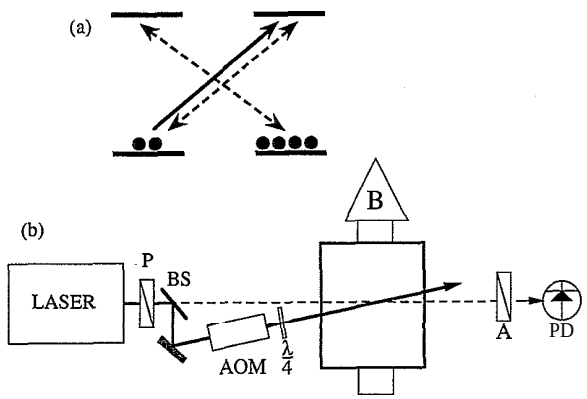

FIG. 1. (a) Typical atomic-level scheme consisting of an electronic $J=\frac{1}{2}\leftrightarrow J'=\frac{1}{2}$ transition. The solid arrow represents the transition interacting with the optical pump beam, the dashed arrows those coupled to the probe beam. (b) Schematic representation of the general experimental setup. The rectangular box in the center represents the atomic vapor cell in the magnetic field ***B***. The pump laser beam (full line) is circularly polarized. A linearly polarized cw laser beam (dashed line) is used for detection of the resulting spin polarization. P represents the polarizer, BS the beam splitter, AOM the acousto-optic modulator, ***B*** the magnetic field, A the analyzer, and PD the photodiode.

While these examples demonstrate that the advantages of optical pumping with modulated light are well known, there is no thorough investigation so far of the dynamics that are induced in the atomic system by the modulated optical field. While such an analysis is crucial for most time-resolved experiments, it is certainly also beneficial for many frequency-domain experiments. The understanding gained from such an analysis allows one, e.g., to compare the advantages of the different modulation schemes, such as harmonic or pulse train modulation for particular experiments.

The possibility of exciting sublevel coherences in systems with very large level splitting cited above is not the only application of modulated optical pumping. In addition, it introduces additional degrees of freedom into the experiment, the most. important ones being frequency and phase of the modulation. These additional degrees of freedom can, e.g., be used to "label" the coherences that are created by the optical irradiation with the corresponding parameter, such as the phase. This labeling scheme makes it possible to follow the evolution of the coherences through an extended experiment. and distinguish coherences created at different stages.

The paper is structured as follows. Section II summarizes first the dynamics occurring in a $J=\frac{1}{2}$ atomic ground state during constant optical pumping. The results are then extended to the case of modulated pumping. In Sec. III, the theoretical results are compared to experimental measurements in Na vapor and some possible applications are discussed. Section IV contains a summary and outlook.

II. THEORY

A. Equation of motion

The goal of this section is the development of a physically intuitive framework that gives a rigorous description of the dynamics occurring in the systems of interest. In order to facilitate this task, we make some assumptions about the system that will be fulfilled in all experimental examples that we present here. We develop the theory for the ground state of a model system with an optically allowed $J=\frac{1}{2}\leftrightarrow J'=\frac{1}{2}$ transition (see Fig. 2) that is homogeneously broadened. The experimental examples will use Na gas with the laser tuned to the D_1 transition and buffer gas added leading to a pressure-broadened homogeneous optical transition and allowing one to neglect excited-state effects and the hyperfine coupling to a good approximation. Since the use of modulated excitation is of interest mainly in those cases where the light intensity is low, we assume that the population of the excited state can be neglected.

Before we start with the analysis of the system under modulated optical pumping, it is helpful to discuss the dynamics of a system irradiated with a laser beam of constant intensity. Several accounts of that situation exist;[2,12] nevertheless, we summarize the situation here in a way that is especially suitable for the understanding of the situation in the case of modulated optical pumping. In addition, our derivation of the equation of motion is more general than those given previously; in particular, it. is also applicable to systems with inequivalent decay rates from the optically excited state to the various ground-state sublevels.

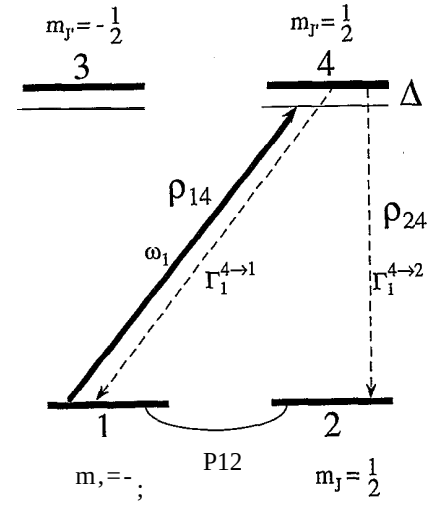

FIG. 2. Level scheme used for the analysis of optical pumping; levels 1 and 2 are substates of the atomic ground state while levels 3 and 4 belong to an electronically excited state. A represents the detuning of the laser frequency from the atomic resonance, $\Gamma_1^{r\to s}$ the spontaneous decay rates, ω_1 the optical Rabi frequency, and ρ_{ij} the elements of the density operator.

Starting from the model system depicted in Fig. 2, the first step is the derivation of equations of motion for the ground-state populations and coherences ρ_{11}, ρ_{12}, and ρ_{22}; the optical coherences and the excited-state populations should not appear in these equations, which, nevertheless should give a correct account of the influence of the optical field. This is of course only possible in the limit of low-power irradiation; in addition, the evolution of the ground-state variables must be slow compared to the decay of the optical coherences. This condition will always be fulfilled in the experiments to be discussed here.

If the atom is irradiated with σ_+ light, the excited-state sublevel $|3\rangle$ is not coupled to the rest of the system, so that it is possible to calculate the full dynamics of the system from a reduced three-level system. We consider, therefore, two electronic ground-state sublevels, one of which couples via the radiation field to an electronically excited state. This three-level system is described by a 3 X 3 density operator. We use the abbreviations

$$x_{ij}=\rho_{ij}+\rho_{ji},\ y_{ij}=i(\rho_{ij}-\rho_{ji}). \tag{1}$$

to describe the dynamics of the system in terms of a set of real-valued variables. The x_{ij} represent, therefore, the real part of the coherence while the y_{ij} correspond to the imaginary part. Physically, they correspond to an induced electric or magnetic dipole moment.

For the time being, we neglect any magnetic fields present and discuss only the influence of the laser field, which is assumed to be a plane traveling wave with angular frequency ω_{las}. Writing $\Gamma_1^{4\to1}$ for the spontaneous decay rate from level 4 to level 1 (see Fig. 2), the equations of motion for the density operator elements in a frame of reference rotating at the frequency of the optical field are

$$
\begin{aligned}
\dot{\rho}_{11} &= (\omega_1/2)y_{14} + \Gamma_1^{4\to 1}\rho_{44} ,\\
\dot{x}_{12} &= (\omega_1/2)y_{24} ,\\
\dot{y}_{12} &= (\omega_1/2)x_{24} ,\\
\dot{\rho}_{22} &= \Gamma_1^{4\to 2}\rho_{44} ,\\
\dot{x}_{14} &= \Delta y_{14} - \Gamma_2 x_{14} ,\\
\dot{y}_{14} &= -\Delta x_{14} - \omega_1(\rho_{11}-\rho_{44}) - \Gamma_2 y_{14} ,\\
\dot{\rho}_{44} &= (-\omega_1/2)y_{14} - \Gamma_1\rho_{44} ,\\
\dot{x}_{24} &= (-\omega_1/2)y_{12} + \Delta y_{24} - \Gamma_2 x_{24} ,\\
\dot{y}_{24} &= (-\omega_1/2)x_{12} - \Delta x_{24} - \Gamma_2 y_{24} ,
\end{aligned}
\tag{2}
$$

where $\Delta = \omega_{14} - \omega_{las}$ represents the offset of the laser frequency from optical resonance and ω_1 the optical Rabi frequency. $\Gamma_1 = \Gamma_1^{4\to 1} + \Gamma_1^{4\to 2}$ is the total decay rate of the excited state and Γ_2 the dephasing rate of the optical coherences.

B. Optical pumping

When the radiation field is switched on initially, the system is in a state of thermal equilibrium. The thermal equilibrium density operator does not commute with the Hamiltonian of the combined system atom plus radiation field; it is therefore forced into a precession and relaxes on a time scale of the order of the optical dephasing time Γ_2^{-1} to a quasistationary state in which the optical coherences are

$$
x_{14} = \rho_{11}\frac{-\omega_1\Delta}{\Delta^2+\Gamma_2^2}, \quad y_{14} = \rho_{11}\frac{-\omega_1\Gamma_2}{\Delta^2+\Gamma_2^2} , \tag{3}
$$

and the population of the excited state is

$$
\rho_{44}(t) = \rho_{11}\frac{\omega_1^2}{2(\Delta^2+\Gamma_2^2)}\frac{\Gamma_2}{\Gamma_1} . \tag{4}
$$

Since the excited state $|4\rangle$ has a finite probability $\Gamma_1^{4\to 2}$ to decay to level 2, which is not coupled to the laser field, population is pumped from level $|1\rangle$ to level $|2\rangle$. In the quasistationary state, this process can be described by a simple rate equation for the populations of the ground-state sublevels:

$$
\frac{d}{dt}\rho_{11}(t) = -k\rho_{11}(t) = -\frac{d}{dt}\rho_{22}(t) , \tag{5}
$$

with the rate constant

$$
k = \Gamma_2\frac{\Gamma_1^{4\to 2}}{\Gamma_1^{4\to 1}+\Gamma_1^{4\to 2}}\frac{\omega_1^2}{2(\Delta^2+\Gamma_2^2)} , \tag{6}
$$

or, in terms of the population difference $z_{12} = \rho_{22} - \rho_{11}$,

$$
\dot{z}_{12} = \frac{d}{dt}(\rho_{22}-\rho_{11}) = 2\dot{\rho}_{11} = k\rho_{11}(t) = k[1 - z_{12}(t)] . \tag{7}
$$

Under the assumptions made here, the ground-state population is therefore pumped completely into the second level. This is of course only valid as long as the relaxation of the ground state can be neglected and no magnetic field is present.

C. Light shift and damping

In addition to the optical pumping, which describes the effect of the optical irradiation on the ground-state populations, the light also affects the ground-state coherences x_{12} and y_{12}. As seen from Eqs. (2), the optical field couples them to the optical coherences x_{24} and y_{24}. As a result, the distinction between ground-state coherences and optical coherences is no longer exact and this partial mixing affects the precession and decay of the ground-state coherences.

From the assumptions made above, the optical coherences are in a quasistationary state on the time scale of the ground-state dynamics, in close analogy to the Born-Oppenheimer approximation for the separation of electronic and nuclear degrees of freedom. As an ansatz for the solution of Eq. (2), we put

$$
x_{12} = \cos(\delta t)e^{-\gamma t}, \; y_{12} = -\sin(\delta t)e^{-\gamma t} , \tag{8}
$$

for the ground-state coherences and

$$
\begin{aligned}
x_{24} &= [-c_1\cos(\delta t) + c_2\sin(\delta t)]e^{-\gamma t} ,\\
y_{24} &= [-c_1\sin(\delta t) - c_2\cos(\delta t)]e^{-\gamma t} ,
\end{aligned}
\tag{9}
$$

for the optical coherences, where δ represents the light shift, i.e., the frequency of the precession caused by the optical field, and γ the associated relaxation rate. Inserting these into the equations of motion, we find the coefficients in the quasistationary regime,

$$
c_1 = 2\delta/\omega_1, \; c_2 = 2\gamma/\omega_1 , \tag{10}
$$

while precession frequency and damping rate are

$$
\delta = \Delta\frac{\omega_1^2}{4(\Delta^2+\Gamma_2^2)}, \quad \gamma = \Gamma_2\frac{\omega_1^2}{4(\Delta^2+\Gamma_2^2)} . \tag{11}
$$

The precession frequency δ corresponds to the well-known light shift. Since the damping rate of the ground-state coherences γ does not depend on the spontaneous emission rates $\Gamma_1^{4\to s}$, it is in general different from the optical pumping rate k, as calculated in Eq. (6). For an isolated $J = \frac{1}{2} \leftrightarrow J' = \frac{1}{2}$ system (e.g., Na atoms), the two rates differ by a factor 1.5 so that the relaxation of the ground-state magnetization is anisotropic; this effect was not discovered in earlier analyses of the situation'* and can give rise to a new type of spin echo. [13] However, under the experimental conditions considered here, with a large pressure broadening, the reorientation of the excited state is generally fast, leading to equal decay rates and accordingly the damping rates for ground-state population difference and coherence become the same.

D. Ground-state dynamics

Having expressed the dynamics of the coherences and populations of the ground state independent of the excited state, it is now possible to reduce the system of interest to the two ground-state sublevels. Since they represent

now our total system of interest, we drop the indices1,2 and expand the density operator and Hamiltonian in terms of the spin operators $\mathbf{S}=(S_x,S_y,S_z)$. The dynamics can be described in a relatively compact way if we define the optical pumping rate $P+$ as

$$P_+=\frac{\omega_1^2}{4\Gamma_2(1+\bar{\Delta}^2)} . \tag{12}$$

With this definition, we can rewrite the light shift δ and damping rate γ as

$$\delta=\bar{\Delta}P_+,\ \gamma=P_+ . \tag{11'}$$

In addition to the effect of the laser field, we include now also the external magnetic field which we take to be oriented along the x axis. The ground-state dynamics are then determined by[1]

$$\dot{\rho}=-i[\mathcal{H},\rho]+\hat{\Gamma}\rho+P_+S_z , \tag{13}$$

$$\mathcal{H}=\bar{\Delta}P_+S_z+\Omega_LS_x , \tag{14}$$

where $\bar{\Delta}=\Delta/\Gamma_2$ represents the resonance offset A of the laser frequency, normalized to the dephasing rate Γ_2 of the optical coherence, $\Omega_L=B\mu_Bg/\hbar$ the Larmor frequency, B the strength of the magnetic field, μ_B Bohr's magneton, and g the Landé factor. $\hat{\Gamma}$ represents the relaxation superoperator that includes all the damping mechanisms summarized above. In the case of fast reorientation of the excited state we have assumed here, the relaxation of all three components is the same and the equation can be simplified to

$$\dot{\rho}=-i[\mathcal{H},\rho]-\gamma_{\text{eff}}\rho+P_+S_z , \tag{13'}$$

with the damping rate $\gamma_{\text{eff}}=\gamma_0+P_+$, where γ_0 summarizes the terms which do not depend on the optical irradiation, such as transit time effects in a gas.

The Hamiltonian is equivalent to a system with a magnetic field

$$\mathbf{\Omega}=(\Omega_L,0,\bar{\Delta}P_+) \tag{15}$$

(written in units of angular frequency), where the x component corresponds to the real magnetic field Ω_L and the light shift $\bar{\Delta}P_+$ appears as a virtual magnetic field along the z axis. The equation of motion can be rewritten in terms of the magnetization vector $\mathbf{m}=(m_x,m_y,m_z)$ whose components are the expansion coefficients of the density operator in the basis (S_x,S_y,S_z):

$$\dot{\mathbf{m}}=\mathbf{\Omega}\times\mathbf{m}-\gamma_{\text{eff}}\mathbf{m}+\mathbf{P} , \tag{16}$$

with $\mathbf{P}=(0,0,P+)$. This equation is quite analogous to the Bloch equation with a magnetic field in the xz plane. The general solution of this equation of motion is[2]

$$\mathbf{m}(t)=\sum_{i=-1}^{1}c_i\xi_ie^{\lambda_it}+\mathbf{m}_\infty , \tag{17}$$

where the eigenvectors ξ_i and eigenvalues λ_i are given as

$$\xi_0=(\Omega_L,0,\bar{\Delta}P_+),\ \lambda_0=-\gamma_{\text{eff}} ,$$

$$\xi_{\pm1}=(\bar{\Delta}P_+,\mp i\Omega,-\Omega_L),\quad \lambda_{\pm1}=\pm i\Omega-\gamma_{\text{eff}} , \tag{18}$$

with

$$\Omega=(\Omega_L^2+\bar{\Delta}^2P_+^2)^{1/2} , \tag{19}$$

and the stationary value is

$$\mathbf{m}_\infty=\frac{P_+}{\gamma_{\text{eff}}(\Omega_L^2+\bar{\Delta}^2P_+^2+\gamma_{\text{eff}}^2)} \times(\bar{\Delta}P_+\Omega_L,-\gamma_{\text{eff}}\Omega_L,\bar{\Delta}^2P_+^2+\gamma_{\text{eff}}^2) . \tag{20}$$

The eigenvector ξ_0 is parallel to the effective field and corresponds thus to longitudinal magnetization, while $\xi_{\pm1}$ describe the transverse component precessing around the effective field. The precession frequency Ω is determined by the Larmor frequency Ω_L and the light-shift term $\bar{\Delta}P_+$. The deviation from the Larmor frequency is always positive and largest if the optical detuning is equal to the homogeneous linewidth($\bar{\Delta}=1$).

The expansion coefficients c_i are determined by the initial condition. For a sample in thermal equilibrium, the ground-state orientation vanishes, i.e, $\mathbf{m}(0)=0$. The coefficients are then

$$c_0=-\frac{\bar{\Delta}P_+^2}{\Omega^2\gamma_{\text{eff}}},\quad c_{\pm1}=\frac{P_+\Omega_L(\pm i\Omega+\gamma_{\text{eff}})}{2\Omega^2(\Omega^2+\gamma_{\text{eff}}^2)} . \tag{21}$$

This solution of the equation of motion [Eqs. (20) and (21)] shows clearly why excitation of sublevel coherence by steady-state irradiation becomes inefficient at large sublevel splittings. This can be understood intuitively by considering that the magnetization is generated in the z direction and undergoes a precession aroung the effective field $\mathbf{\Omega}$. For large sublevel splittings, $|\Omega_L|\gg|\bar{\Delta}P_+|$, the direction of the effective field is orthogonal to the z axis so that the precession leads to destructive interference between magnetization packages created at different times.

E. Modulated excitation

This destructive interference can be shown easily if the concept of different packets of magnetization being created at different times during the experiment is carried over into an actual experiment. Figure 3 shows an example where a sequence of short pulses was used to excite the magnetization (for experimental details see Sec. III or Ref. 2). In the top trace, the pulse spacing is equal to the Larmor period, so that the different magnetization packets are generated in phase and interfere constructively. In the second trace, the pulse spacing is equal to 3 times the Larmor period; the various packets still interfere constructively, but the total amplitude is smaller since the number of pulses per unit of time is three times smaller than in the top trace so that less magnetization is generated. In the third trace, the pulse spacing is equal to half the Larmor period; successive packets are therefore exactly out of phase and interfere destructively. The remaining magnetization is due to the fact that the magnetization is damped before the next packet is created.

The destructive interference between packets of magnetization created at different times is the basic motivation for using modulated excitation: If the magnetization is not generated continuously, but in packages, it be-

comes possible to create them in phase, so that the interference between them becomes constructive. This modulated optical pumping can be implemented in different ways, via modulation of the polarization or intensity of the light. As a specific example we discuss here the case of harmonic modulation of the laser intensity. This scheme allows a straightforward theoretical analysis and its experimental implementation gives a large amount of freedom in the variation of the relevant parameters such as frequency, phase, and amplitude of the modulation.

With the sinusoidal modulation scheme, the optical pumping rate for our model system becomes time dependent and can be written as

$$P_+(t)=2P_0[\,1+\cos(\omega_m t-\phi)]\,,$$

where ω_m represents the frequency and ϕ the phase of the modulation. The time-dependent Hamiltonian for the two-level system can then be written as

$$\mathcal{H}(t)=\Omega_L S_x + S_z 2\delta_0[\,1+\cos(\omega_m t-\phi)]\,, \tag{22}$$

where $2\delta_0=2\bar{\Delta}P_0$ represents the average light shift. The equation of motion is then

$$\frac{d\rho}{dt}=-i[\mathcal{H}(t),\rho]-\gamma_{\rm eff}(t)\rho+P_+(t)S_z\,. \tag{23}$$

We are now especially interested in the case of low-power excitation, when the optical pump rate is small compared to the sublevel splitting. In this case, it is useful to transform the time-dependent equation of motion into a frame of reference rotating at the modulation frequency ω_m:

$$\frac{d\rho^r}{dt}=-i[\mathcal{H}^r(t),\rho^r]-\gamma_{\rm eff}(t)\rho^r+P(t)S_z^r\,, \tag{24}$$

where the superscript indicates that the operators are to be transformed into the rotating reference frame. The transformation can be accomplished by

$$\rho^r(t)=U(t)\rho(t)U^{-1}(t)\,, \tag{25}$$

$$U(t)=e^{i\omega_m t S_x}\,, \tag{26}$$

$$\begin{aligned}\mathcal{H}^r(t)&=U(t)\mathcal{H}(t)U^{-1}(t)-\dot{U}(t)U^{-1}(t)\\&=\delta_L S_x+\delta_0 S_z[\cos(\phi)+2\cos(\omega_m t)\\&\qquad+\cos(2\omega_m t-\phi)]\\&\quad+\delta_0 S_y[\sin(\phi)+2\sin(\omega_m t)+\sin(2\omega_m t-\phi)]\,.\end{aligned} \tag{27}$$

Here, $\delta_L=(\Omega_L-\omega_m)$ represents the difference between the sublevel splitting Ω_L and the modulation frequency ω_m. On a time scale long compared to the precession frequency, the modulated terms can be neglected in first order. This corresponds of course to a rotating-wave approximation: only the terms corresponding to the correct velocity and sense of rotation are retained. The Hamiltonian becomes then

$$\mathcal{H}^r(t)=\delta_L S_x+\delta_0[S_z\cos(\phi)+S_y\sin(\phi)]\,. \tag{28}$$

This Hamiltonian is quite similar to the one describing the excitation of sublevel coherence with unmodulated light. The main differences are that the field due to the sublevel splitting is reduced by the modulation frequency and therefore can be made to vanish and that the light-shift contribution to the field is no longer parallel to the z axis but can be made to point in any direction in the yz plane by appropriate choice of the modulation phase. Via a combination of the two parameters, frequency and phase, it is therefore possible to generate an effective field pointing in an arbitrary direction in the rotating frame.

Since we have assumed here that the relaxation term in Eq. (24) is isotropic, the transformation into the rotating frame is simply achieved by averaging the relaxation rate over time. For the above modulation scheme we therefore obtain the result $\gamma_{\rm eff}=\gamma_0+2P_0$.

In addition to the transformation of the Hamiltonian, the pumping term also has to be transformed as

$$\begin{aligned}P(t)S_z^r=P_0\{&S_z[\cos(\phi)+2\cos(\omega_m t)+\cos(2\omega_m t-\phi)]\\&+S_y[\sin(\phi)+2\sin(\omega_m t)+\sin(2\omega_m t-\phi)]\}\,.\end{aligned} \tag{29}$$

We may again neglect the time-dependent terms so that

$$P(t)S_z^r\approx P_0[S_z\cos(\phi)+S_y\sin(\#)]\,. \tag{30}$$

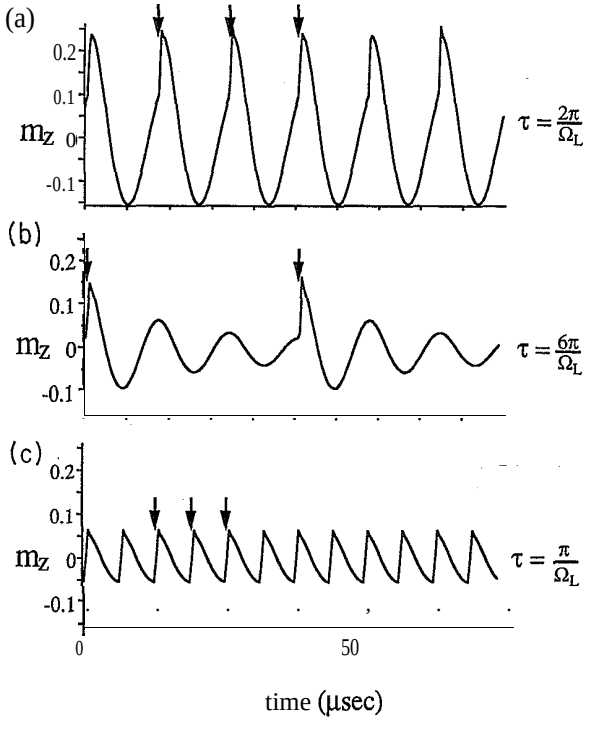

FIG. 3. Measured evolution of magnetization as a function of time for various pulse spacings; the arrows indicate the position of a representative set of pulses. In the top trace, the pulse spacing τ is equal to the Larmor period, in the second trace 3 times the Larmor period, and in the third trace half the Larmor period. For details of the experimental setup see Sec. III.

The orientation of the magnetization generated by the optical pumping therefore can also be varied by changing the modulation phase. A phase shift is therefore equivalent to changing the orientation of the rotating frame.

An interesting result of this transformation into the rotating frame is that with the modulation scheme chosen here, the pumping rate is at most half the size of the relaxation rate so that the stationary magnetization is always below $\frac{1}{2}$. Higher ratios of pumping rate to relaxation rate, and correspondingly higher polarizations, could be obtained with different modulation schemes, e.g., via modulation of the polarization of the pump field.

F. Evolution

As this derivation shows, the equation of motion for the system is quite analogous to that obtained with unmodulated light if the dynamics are calculated in a frame of reference rotating at the modulation frequency. If we redefine the nutation frequency as $\Omega=(\delta_L^2+\delta_0^2)^{1/2}$ and $\gamma_{\rm eff}=\gamma_0+2P_0$, we therefore can use the results obtained in earlier work[1-3] to calculate the evolution of the system in the rotating frame. As a specific example, we calculate the evolution of the magnetization during a one-pulse experiment. We assume that the system is initially in thermal equilibrium ($\mathbf{m}=0$) and a modulated pulse is switched on at $t=0$ with phase $\phi=0$ for a duration T. The evolution of the magnetization in the rotating frame is then

$$m_{yz}(t)=\frac{P_0}{\gamma_{\rm eff}}[m_{yz\infty}+m_{yzl}+m_{yzt})e^{-\gamma_{\rm eff}t}], \tag{31}$$

where

$$m_{yz\infty}=\frac{1}{\Omega^2+\gamma_{\rm eff}^2}\{\delta_L\gamma_{\rm eff},\delta_0^2+\gamma_{\rm eff}^2\} \tag{32}$$

represents the stationary value,

$$m_{yzl}=\left\{0,-\frac{\bar{\Delta}^2P_0^2}{\Omega^2}\right\}, \tag{33}$$

the component parallel to the effective field, and

$$m_{yzt}=\frac{\delta_L\gamma_{\rm eff}}{\Omega^2(\Omega^2+\gamma_{\rm eff}^2)}(\Omega^2+\gamma_{\rm eff}^2)^{1/2} \times\{\Omega\cos(\Omega t-\alpha),\delta_L\sin(\Omega t-\alpha)\} \tag{34}$$

the transverse component precessing around the effective field. The phase a is given as

$$\tan\alpha=-\gamma_{\rm eff}/\Omega. \tag{35}$$

Equations (31)–(35) describe the evolution of the magnetization in the rotating frame during the pulse. If the pump field is switched off at a time T, after the system has reached the stationary state, a free-induction decay occurs:[3]

$$m_{yz}(t)=\{-A\sin[\delta_L(t-T)+\beta],A\cos[\delta_L(t-T)+\beta]\}e^{-\gamma_0(t-T)}, \tag{36}$$

where amplitude A and phase β are given as

$$A=[m_y(T)^2+m_z(T)^2]^{1/2} =\frac{P_+}{\gamma_{\rm eff}}\frac{[\gamma_{\rm eff}^2\delta_L^2+(\delta_0^2+\gamma_{\rm eff}^2)^2]}{\delta_L^2+\delta_0^2+\gamma_{\rm eff}^2}, \tag{37}$$

$$\tan\beta=-\frac{m_y(T)}{m_z(T)}=\frac{\gamma_{\rm eff}\delta_L}{\delta_0^2+\gamma_{\rm eff}^2}. \tag{38}$$

These two transient effects are summarized in Fig. 4, where the evolution of both magnetization components is shown: when the laser is switched on, magnetization is generated by the optical pulse and starts to precess around the effective field with the nutation frequency Ω. After a few oscillations, the system settles into a steady state determined by Eq. (32); under the relatively weak pump field chosen for this example, the stationary magnetization is closer to the y axis than to the z axis. When the laser is turned off, the magnetization starts to precess again, this time around the x direction. In the absence of optical pumping, the magnetization now decays to zero.

G. Detection

The polarization-selective detection of a transmitted probe laser beam that is initially linearly polarized leads to a difference signal that is either proportional to the dispersion or the-absorption of the unpolarized medium and the component of the magnetization $m_z^l(t)$ parallel to the laser beam,[2,3] measured in the laboratory coordinate system. The setups for both cases are shown in Fig. 5,

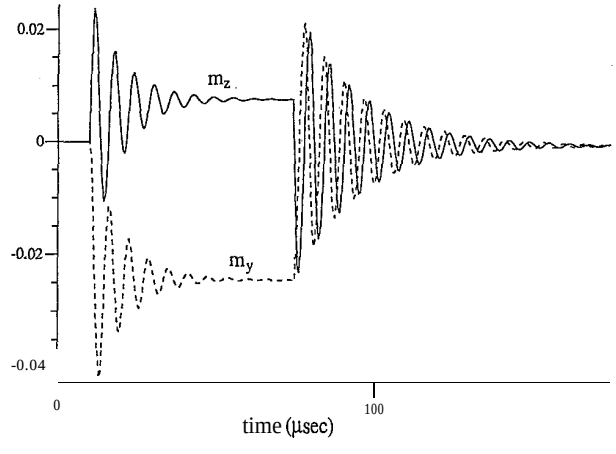

FIG. 4. Calculated evolution of the magnetization in the rotating frame. The full line represents the z component; the dashed line the y component. Parameters: $\delta_L/2\pi=160$ kHz, $\bar{\Delta}=3$, $P_0=5\times10^4\text{sec}^{-1}$, and $\gamma_0=5\times10^4\text{sec}^{-1}$.

with the $\lambda/4$ plate being present in the case of absorptive detection and absent in the dispersive case.

In order to calculate the observed signal, we have to transform the yz component of the magnetization back into the laboratory frame. This transformation is achieved by

$$m_z^l(t)=m_z(t)\cos(\omega_m t)-m_y(t)\sin(\omega_m t)\ , \tag{39}$$

where the upper index l refers to the laboratory frame of reference, while the rotating-frame components carry no index. During the initial transient, the signal is therefore proportional to

$$m_z^l(t)=\frac{P_0}{\gamma_{\rm eff}}\{[m_{z\infty}\cos(\omega_m t)+m_{y\infty}\sin(\omega_m t)]+m_{yzl}\cos(\omega_m t)e^{-\gamma_{\rm eff}t}$$
$$+m_{yzt}[\Omega\cos(\Omega t-\alpha)\sin(\omega_m t)+\delta_L\sin(\Omega t-\alpha)\cos(\omega_m t)]e^{-\gamma_{\rm eff}t}\}\ . \tag{40}$$

We eliminate the products of angles in the third term to get

$$m_z^l(t)=\frac{P_0}{\gamma_{\rm eff}}([m_{z\infty}\cos(\omega_m t)+m_{y\infty}\sin(\omega_m t)]+m_{zl}\cos(\omega_m t)e^{-\gamma_{\rm eff}t}$$
$$+m_{yzt}\tfrac{1}{2}\{(\Omega+\delta_L)\sin[(\omega_m+\Omega)t-\alpha]-(\Omega-\delta_L)\sin[(\omega_m-\Omega)t-\alpha]\}e^{-\gamma_{\rm eff}t})\ . \tag{41}$$

The resulting signal oscillates, therefore, at the modulation frequency ω_m, with sidebands occurring at $\omega_m\pm\Omega$. During the FID, the signal is calculated analogously as

$$m_z^l(t)=-A\cos[\delta_L(t-T)+\omega_m t+\beta]e^{-\gamma_0(t-T)}\ . \tag{42}$$

It oscillates, therefore at the single frequency $\omega_m+\delta_L$. This signal is obtained by a straightforward polarization-selective measurement of the transmitted light, However, inspection of Eq. (39) suggests an alternative: if phase-sensitive detection at the modulation frequency is used, the (trivial) contribution of ω_m can be eliminated from the signal and the measurement reflects directly the evolution of the corresponding quantities in the rotating frame. If a two-channel device is used, both m_z and m_y can be measured simultaneously as the in-phase and out-of-phase components. The phase-sensitive signal corresponds, therefore, directly to the signal calculated above and shown in Fig. 4.

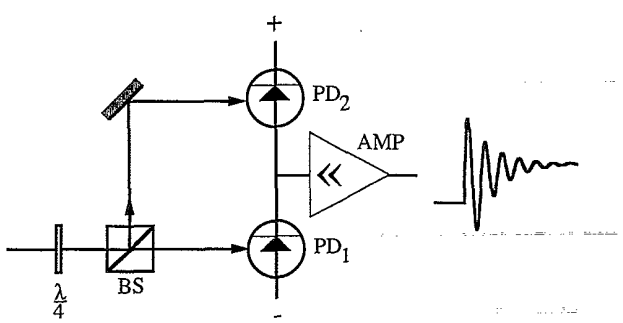

FIG. 5. Setup for the polarization selective detection of the transmitted light. If the observed signal is to be proportional to the absorption of the unpolarized sample, the $\lambda/4$ plate is present, for a dispersive measurement it is absent. BS represents *the* polarizing beam splitter, PD the photodiode, and AMP the amplifier.

H. Pulse train modulation

The results obtained in the previous sections now also allow a comparison of the different modulation schemes. While we have assumed sinusoidal modulation of the laser intensity for the calculation, it is obvious how this result can be generalized to other modulation schemes: the dynamics should always be analyzed in a rotating frame of reference where the time-dependent terms can be neglected. If the modulation is not harmonic, such as in the case of pulse train excitation, there are many possibilities for the choice of the rotating frame, the rotation speed corresponding to the different frequency components of the pulse train. For the idealized case of a train of &function pulses, the laser intensity can be written as

$$I(t)=I_0\sum_{i=0}^{\infty}\cos\left[\frac{i2\pi t}{\tau}\right]\ , \tag{43}$$

where τ represents the pulse spacing. In general, only one of the harmonics of the repetition rate corresponds to a resonance. As an example, the hyperfine splitting of the Cs ground state was measured with the 110th harmonic of the pulse repetition rate.' The transformation to the rotating frame is then achieved by the unitary transformation

$$U(t)=\exp\left[\frac{n2\pi}{\tau}1\right], \tag{44}$$

where n represents the index of the harmonic.

Since the light source for pulse train modulation schemes is often a pulsed laser with high peak intensity, it is necessary to discuss the validity of our assumption that the atomic system is only weakly pumped. As a specific example, we consider an experiment with a mode-locked laser system and picosecond pulses.' The high peak power of these pulses clearly violates the weak pumping assumption; however, in most cases the pulse repetition

rate is slow compared to the dephasing time Γ_2 of the optical coherences. In those cases it is therefore permissible to use the low-intensity approximation as long as the mean power of the pump beam does not exceed the saturation intensity of the atomic system. Apart from the intensity, pulsed laser sources have a larger spectral width than cw lasers; this can be incorporated into our formalism, e.g., by including the spectral width of the laser field in the optical dephasing rate Γ_2.

If the different modulation schemes are to be compared, one main difference is apparently that in the case of pulse train excitation, all the magnetization created during an experiment adds coherently if a harmonic of the pulse repetition rate coincides with the precession frequency of the sublevel coherence. In the case of harmonic modulation, however, only $\frac{1}{2}$ of the average incident laser intensity ($\frac{1}{4}$ of the maximum intensity) acts as pump field in the rotating frame [see Eq. (30)]. Judging by the criterion of utilization of the incident light, the pulse train modulation is, therefore, clearly more efficient. However, if the highest possible pump rate in the rotating frame at a given peak power is the criterion, the harmonic modulation scheme performs better. Other criteria that will affect the comparison are, e.g., the desirability of multiple resonances (different harmonics of the pulse repetition rate), the ability to adjust the modulation frequency, and other experimental considerations.

III. EXPERIMENTAL RESULTS

The general experimental setup (see Fig. 1) used for experiments on optically induced sublevel coherences has been described in detail elsewhere.[2] The atomic medium was again Na vapor and Ar was used as a buffer gas. For the experiments discussed here, the modulation of the pump laser intensity is achieved in the same way as the generation of the pulses, by an acousto-optic modulator (AOM) (see Fig. 6). The radio frequency is gated with the desired pulse shape and the resulting electrical signal is applied to the driver of the acousto-optic modulator. The signal can be measured directly at the detector (signal path 1 in the figure) or after phase-sensitive detection (path 2), in which case the reference is obtained from the same source that is used to drive the acousto-optic modulator. For most experiments discussed here, the laser frequency was set on resonance with the Na D_1 transition, the pump laser power was set to an average power of 0.9 mW and the beam diameter was 1.1 mm; under these conditions, the effective optical pump rate P_0 was $1.2\times10^4\,\mathrm{sec}^{-1}$.

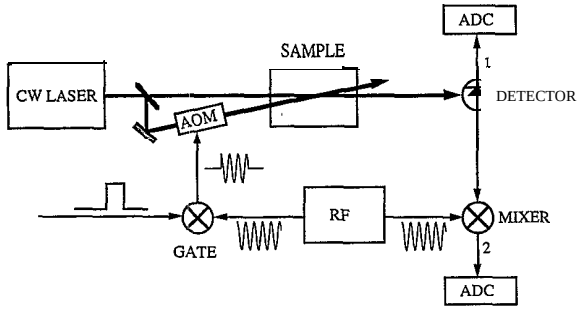

FIG. 6. Modification of the general experimental setup for modulated excitation. The different signal paths for direct and phase-sensitive detection are labeled 1 and 2, respectively. For details see text.

A typical experimental signal is shown in Fig. 7: the top trace represents the time dependence of the pump laser intensity, the second trace the directly detected signal, and the bottom trace was obtained with phase-sensitive detection. As can be seen, the system moves towards a pseudostationary state in which the signal oscillates at the modulation frequency. This oscillation corresponds of course to the driven precession of the magnetization around the effective field, synchronously with the modulated intensity of the pump laser. This can be seen most easily in the third trace, which was obtained with phase-sensitive detection. The beat frequency visible here is the difference between the free precession frequency of the system and the modulation frequency. When the pump laser is switched off, the system starts to precess freely and a FID signal appears.

While the information content of the demodulated signal is basically the same as that of trace (b), the analysis is clearly simplified. The features of the signal are the same as those of a low-field system excited with a dc pulse. This allows one to compare the experimental results directly with the dynamical calculations performed in the rotating frame. The details of the initial and final tran-

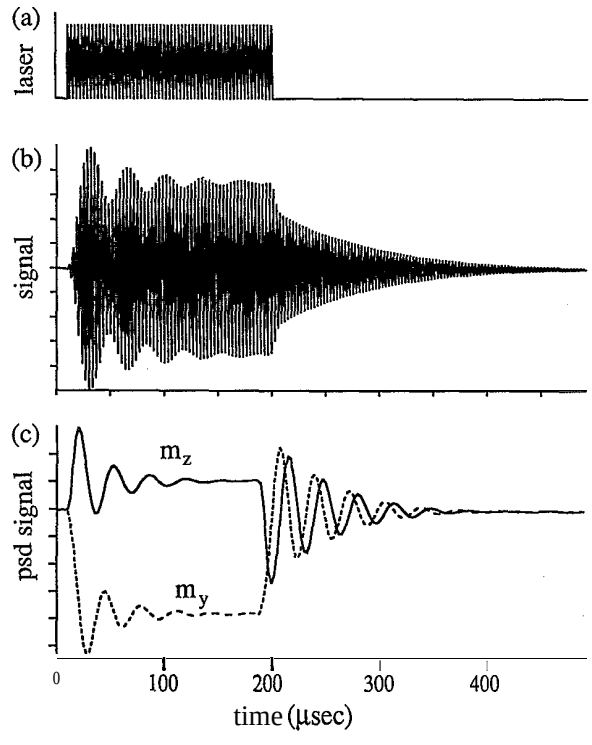

FIG. 7. (a) Intensity of the pump beam as a function of time, (b) together with the resulting signal. (c) The bottom trace shows the same signal, using phase-sensitive detection at the modulation frequency. Parameters: $\delta_L/2\pi = 328$ kHz, pump laser intensity $= 0.9\,\mathrm{mW\,mm}^{-2}$.

sients are completely analogous to those obtained with dc pulses.[2,3] As can be seen from Fig. 7, the phase-sensitive detection simplifies the data analysis by removing the oscillations due to the driving field from the signal. In addition, since the frequency range of the demodulated signal can be considerably smaller than that of the original signal, this procedure has also the advantage that the requirements on the speed of the analog-to-digital converters are also reduced.

In the bottom trace of Fig. 7, the full line corresponds to the in-phase output of the phase-sensitive detector, while the dashed line corresponds to the out-of-phase component. According to Eq. (39), they should correspond to the z and y components of the magnetization in the rotating frame, respectively. A single measurement yields therefore, not only the component of the magnetization parallel to the probe beam (m_z), but also the component orthogonal to probe beam and magnetic field (m_y). In Fig. 8, both components are measured for various modulation frequencies. Clearly m_z has an absorptionlike dependence on the offset of the modulation frequency, i.e., it reaches a maximum if the modulation frequency is equal to the Larmor frequency and does not depend on the sign of the offset. m_y, on the other hand, has a dispersionlike (antisymmetric) offset dependence.

It was shown earlier[3] that the stationary value of the magnetization should have a Lorentzian dependence on the field strength. With the current setup this behavior can be measured, by tuning the modulation frequency to both sides of the Larmor frequency. In Fig. 9, the stationary values of m_y and m_z were measured systematically and compared to the theoretical absorption and dispersion line shapes. The agreement between the theoretical and the observed dependence is excellent. The width of the resonance line equals 7 kHz and is determined primarily by the diffusion rate γ_0 at which the atoms traverse the laser beam.

In an earlier work using dc pulses for excitation of sublevel coherence,[3] it was shown that amplitude and phase of the FID signal depend strongly on laser intensity, laser detuning, and magnetic-field strength. In light of the present investigations, it is clear that this behavior can be understood as a detuning effect: in the case of dc excitation, the detuning is equal to the Larmor frequency of the system. The amplitude and phase dependence found in the earlier work can be generalized, therefore, to the present situation if the Larmor frequency is replaced with the resonance detuning.

In order to illustrate this dependence on the resonance offset, Fig. 10 shows the Fourier transforms of the FID signal as a function of the modulation frequency. They correspond to conventional magnetic resonance spectra excited with an off-resonant radio-frequency pulse. Between successive traces, the modulation frequency (and therefore the carrier frequency for the demodulation) was shifted by 4 kHz. Since the Larmor frequency remains constant, the resonance line is shifted by the same amount in the opposite direction. As expected, the amplitude reaches a maximum if the modulation frequency matches the Larmor frequency and falls off to both sides. The phase of the FID and of its Fourier transform and

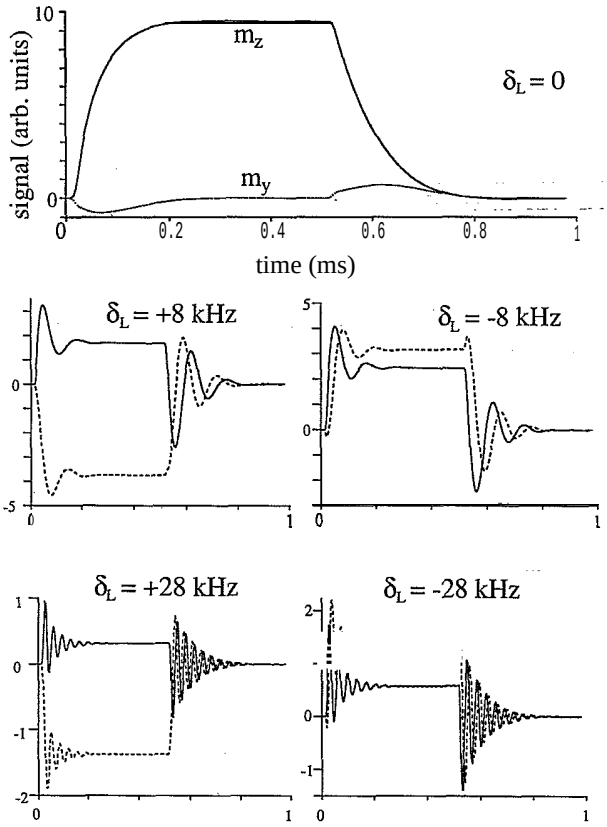

FIG. 8. Phase-sensitive detection of magnetization for various detunings δ of the modulation frequency. The full line corresponds to the in-phase component m_z; the dashed line to the out-of-phase component m_y.

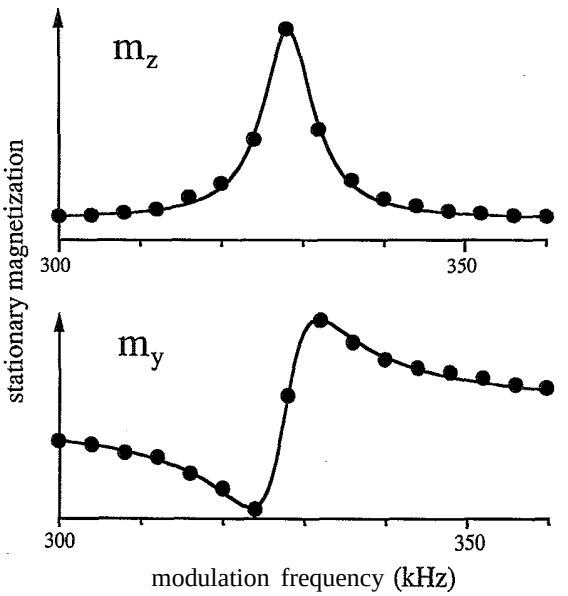

FIG. 9. Stationary magnetization, in and out of phase with the modulation as a function of the modulation frequency. The parameters for the theoretical curves are half-width equals 3.8 kHz and resonance frequency equals 328 kHz.

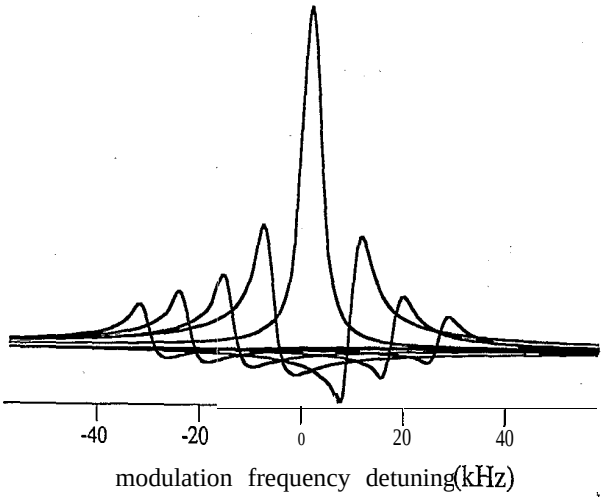

FIG. 10. Fourier transform of the FID as a function of the modulation frequency detuning δ. Phase-sensitive detection at the modulation frequency was used, so that the center frequency of the resonance appears at the corresponding detuning.

falls off to both sides. The phase of the FID and of its Fourier transform corresponds to the prediction of Eq. (38). The physical interpretation of this formula is quite simple if one considers the special case of optically resonant excitation ($\Delta=0$). Equation (38) simplifies then to $\tan\beta=\delta_L/\gamma_{\text{eff}}$. The phase can be understood, therefore, as the precession angle that the magnetization acquires at the precession frequency δ_L during the phase-memory time γ_{eff}^{-1}.

As in the case of dc pulse excitation, the observed signal depends not only on the resonance detuning, but also on the laser intensity. Experimental results are presented in Fig. 11 together with the theoretical prediction which was calculated without any adjustable parameters, apart from the vertical scaling. Note that the system is almost completely polarized even at the relatively low pump power of 17 mW.

As we have emphasized above, the modulation of the laser intensity introduces also additional degrees of freedom into the experiment, such as frequency and phase of the modulation. These additional variables can, e.g., be used to "label" the sublevel coherence generated in the optical pumping process. As we have seen above, a change in the phase of the modulation leads to the magnetization being generated in a different direction in the rotating frame.

Figure 12 shows an example of the application of such a phase-shifting scheme: in a two-pulse experiment (see first trace), the phase of the modulation of the first pusle was incremented systematically while it was kept constant during the second pulse. The subsequent traces show details of the signal for three different excitation phases; the dashed lines connect equal times and are intended as guides to the eye. During and after the first pulse, the observable signal follows the phase of the excitation, i.e., it evolves as $\cos(\delta_L t-\phi)$, as can be verified by comparing the signal in the vicinity of the dashed reference line: in the first trace, the reference line goes

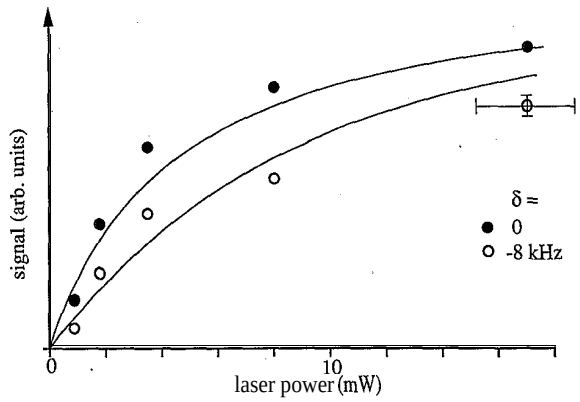

FIG. 11. Stationary magnetization as a function of laser power with the modulation frequency set on resonance (full circles) and at a detuning of $\delta=-8$ kHz (open circles) of the modulation frequency.

through a signal maximum, in the second trace the signal is approximately zero, and in the bottom trace a minimum. By contrast, the magnetization created by the second pulse is independent of the phase of the modulation during the first. In this experiment, an inhomogeneous magnetic field was used, so that the coherences created by the pulses decayed rapidly and inhomogeneously. The second pulse led therefore to an echo with the time between the second pulse and the echo maximum equal to the delay between the two pulses. The echo is formed by magnetization generated during the first pulse which therefore "remembers" the phase. Due to the phase reversal associated with the echo formation, it appears with the inverse sign of the first FID, evolving as $\cos(\delta_L t+\phi)$, where ϕ is again the modulation phase. This example shows that the modulation phase can be used as a label for the coherence created during the optical pumping process. Details of the experiment will be published elsewhere.[14]

IV. CONCLUSION

Modulation of the intensity of the optical field has several attractive features: it allows one to pump atomic

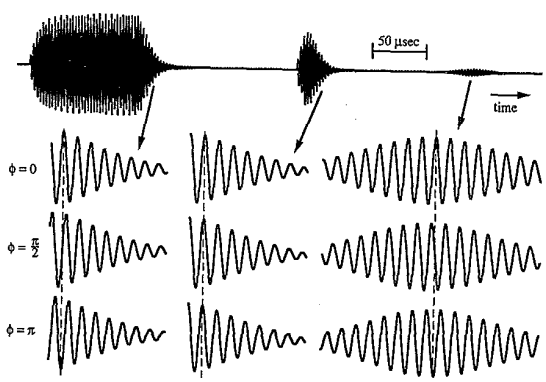

FIG. 12. "Labeling" of coherences by the phase of the modulation. The top trace shows a typical signal of a two-pulse experiment; the lower traces show the first and second FID and the echo for three different phases of the first pulse.

systems optically under conditions where pumping with a constant intensity is no longer possible, e.g., due to a large level splitting. The modulation affects not only the optical pumping, but equally the fictitious fields_ generated by the light-shift effect. If modulated excitation is used, the dynamics occur effectively in a frame of reference rotating around the direction of the magnetic field; in this reference frame, the static magnetic field is reduced by $(\omega_m \hbar)/(\mu_B g)$. This reduction of the strength of the static field represents an additional degree of freedom that allows the experimenter to change the apparent field during the experiment by adjusting the modulation frequency. In most cases, the experimenter will set the modulation frequency near the Bohr frequency of the system in order to make the excitation dynamics most efficient. Such a procedure allows one to effectively turn off the evolution of the sublevel coherences during the preparation step; when the preparation of the system into the desired initial condition is complete, the laser can be turned off and free precession is allowed to proceed.

A second degree of freedom that is added by this procedure is the phase of the modulation. This can be used, e.g., to change the dynamics of the system in an experiment with more than one pulse. Alternatively it can be considered as a label of the coherence created by the pulse. An application of this method is the labeling of multiple quantum coherence described elsewhere. [13]

The introduction of a harmonic time dependence into the experiment and the fact that the most natural frame of reference for the description of the dynamics rotates with respect to the laboratory frame at the modulation frequency suggest the use of phase-sensitive detection. This allows also a reduction of the size of the data set and, if it is performed with analog electronics, the requirements on the speed of the analog-to-digital conversion are significantly reduced. In addition, it is possible to detect the in-phase and out-of-phase components separately, thereby simplifying the data analysis.

The results presented here show that the reduction of the amplitude of sublevel coherence created by optical pulses under conditions of long-pulse excitation can be understood as an off-resonance effect: the intensity of the optical field is constant during the pulse and therefore off resonance with respect to the Bohr frequency of the coherence generated. The modulation changes this by allowing the experimenter to move the excitation frequency from 0 to a value near the Bohr frequency. With techniques available today, modulation frequencies up into the GHz range are feasible and it seems likely that the technology even will be improved in the future. Even higher modulation frequencies are, of course, possible by superposition of light from two separate lasers; however, with such a setup, the resolution of the resulting spectra is determined by the laser linewidths and not by the coherence properties of the radio frequency, as in the present case.

ACKNOWLEDGMENTS

This work was supported by the Schweizerischer Nationalfonds.

[1] See, e.g., D. Suter and J. Mlynek, in *Advances in Magnetic and Optical Resonance,* edited by W. S. Warren (Academic, New York, in press), Vol. 16, and references therein.
[2] D. Suter, M. Rosatzin, and J. Mlynek, Phys. Rev. A 41, 1634 (1990).
[3] M. Rosatzin, D. Suter, and J. Mlynek, J. Opt. Soc. Am. B 7, 1231 (1990).
[4] I. A. Walmsley, M. Mitsunaga, and C. L. Tang, Phys. Rev. A 38.4681 (1988).
[5] W. E. Bell and A. L. Bloom, Phys. Rev Lett. 6,280 (1961).
[6] J. Mlynek, K. H. Drake, G. Kersten, D. Frölich, and W. Lange, Opt. Lett. 6, 87(1981).
[7] T. Mishina, Y. Fukuda, and T. Hashi, Opt. Commun. 66, 25 (1988).
[8] H. Harde and H. Burggraf, Opt. Commun. 40, 441 (1982).
[9] H. Lehmitz, W. Kattau, and H. Harde, in *Methods of Laser Spectroscopy,* edited by Y. Prior, A. Ben-Reuven, and M. Rosenbluh (Plenum, New York, 1986), p. 97.
[10] M. Tanigawa, Y. Fukuda, T. Kohmoto, K. Sakuno, and T. Hashi, Opt. Lett. 8, 620 (1983); T. Mishina, M. Tanigawa, Y. Fukuda, and T. Hashi, Out. Commun. 62. 166 (1987).
[11] M. Rosatzin, D. Suter, and J. Mlynek, Phys. Rev. A 42, 1839 (1990).
[12] F. Mitschke, R. Deserno, W. Lange, and J. Mlynek, Phys. Rev. A 33, 3219 (1986).
[13] M. Rosatzin, Ph.D. thesis, Eidgenössische Technische Hochschule Zürich, Ziirich, 1990.
[14] D. Suter, M. Rosatzin, and J. Mlynek (unpublished).